Electrochimica Acta 231 (2017) 713–720

Contents lists available at ScienceDirect

Electrochimica Acta

journal homepage: www.elsevier.com/locate/electacta

W@Au Nanostructures Modifying Carbon as Materials for Hydrogen Peroxide Electrogeneration

Vanessa S. Antonin[a], Luanna S. Parreira[a], Luci R. Aveiro[a], Fernando L. Silva[b], Ricardo B. Valim[b], Peter Hammer[c], Marcos R.V. Lanza[b], Mauro C. Santos[a,*]

[a] LEMN – Laboratório de Eletroquímica e Materiais Nanoestruturados – CCNH – Centro de Ciências Naturais e Humanas, UFABC – Universidade Federal do ABC, CEP 09210-170, Santo André, SP, Brazil
[b] Instituto de Química de São Carlos, USP – Universidade de São Paulo, Caixa Postal 780, CEP 13560-970, São Carlos, SP, Brazil
[c] Instituto de Química, UNESP – Universidade Estadual Paulista, CEP 14800-900, Araraquara, SP, Brazil

ARTICLE INFO

Article history:
Received 20 September 2016
Received in revised form 16 December 2016
Accepted 28 January 2017
Available online 11 February 2017

Keywords:
Hydrogen peroxide electrogeneration
oxygen reduction reaction
core-shell
W@Au

ABSTRACT

In this work, materials based on core-shell W@Au type structures were found to have promise for use as electrocatalysts on the *in-situ* production of H_2O_2 by means of the oxygen reduction reaction (ORR). We describe herein the synthesis and characterization of these materials and then present a study of electrocatalytic activity towards ORR by the electrogeneration of H_2O_2 employing these materials supported on Vulcan XC-72R carbon corresponding to 1 and 2 wt% loading. The use of W@Au/C materials led to higher activity compared to pure carbon and commercial Pt/C, and the optimal load is 1%, which presented the highest ring current for the ORR using the rotating ring-disk electrode technique. Exhaustive electrolysis using a W@Au/C 1% gas diffusion electrode (GDE) was employed to verify the real amount of H_2O_2 electrogenerated comparing with a Vulcan XC-72R GDE. We verified that the W@Au/C 1% material is able to generate 50% more H_2O_2 than carbon. These results can be explained based on synergistic interactions presented by the W@Au/C 1% material and also by both conductivity and hydrophilicity differences provided by the nanostructures supported on carbon.

1. Introduction

As an essential resource to life, water must be continually purified. Currently, water pollution is a major global problem that requires treatment planning and urgent solutions. In this context, advanced oxidation processes (AOPs) are good alternatives to be applied on the degradation of hazardous pollutants, such as pharmaceuticals [1–3], dyes [4,5], and herbicides [6,7], among other organic compounds found in groundwater, surface water and industrial wastewater.

AOPs are characterized by chemical oxidation reactions mediated by the *in-situ* generation of the hydroxyl radical (•OH), an extremely reactive and low selective species. The standard reduction potential of the hydroxyl radical ($E^\circ(^\bullet OH/H_2O) = 2.80$ V/SHE) makes this radical a very powerful and non-selective oxidizing agent, reacting with organic species to give hydroxylated or dehydrogenated derivatives until their complete mineralization (transformation into CO_2, water and inorganic ions). The hydroxyl radicals are formed using oxidizing agents, such as H_2O_2 and O_3, and the efficiency of these reactions can be increased by the combination with an additional irradiation source and/or catalysts (metal ions, semiconductors) [8–11].

The anthraquinone oxidation (AO) method is widely used in the large-scale production of hydrogen peroxide, even though it involves multiple steps, high energy consumption and waste discharge [12,13]. Recently, *in situ* H_2O_2 generation of hydrogen peroxide has gained increasing attention because it reduces costs and prevents potential risks in the transportation, storage, and handling of concentrated H_2O_2 [14]. Furthermore, H_2O_2 decomposes into non-contaminating products (friendly environmental products), such as water and oxygen [13,15].

Electrochemical technology can be employed in the *in situ* generation of H_2O_2 in aqueous medium at concentrations reaching up to hundreds of milligrams per liter [16,17]. However, the oxygen reduction reaction (ORR) can be performed at the cathode and can generate different products via two different pathways: (i) the two-electron pathway, forming hydrogen peroxide or hydroperoxide ion (HO_2^-) (which is the H_2O_2 conjugated base) and (ii) the

* Corresponding author. Tel.: +55 11 4996 0163; fax: +55 11 4996 0090.
E-mail addresses: mauro.santos@ufabc.edu.br, drmcsa@gmail.com (M.C. Santos).

http://dx.doi.org/10.1016/j.electacta.2017.01.192
0013-4686/

four-electron pathway, which forms water or hydroxyl groups, depending on the pH of the solution.

i. Alkaline solutions.

$$O_2 + H_2O + 2e^- \rightarrow HO_2^- + OH^- \quad (1)$$

Acid solutions.

$$O_2 + 2H^+ + 2e^- \rightarrow H_2O_2 \quad (2)$$

ii. Alkaline solutions.

$$O_2 + 2H_2O + 4e^- \rightarrow 4OH^- \quad (3)$$

Acid solutions.

$$O_2 + 4H^+ + 4e^- \rightarrow 2H_2O \quad (4)$$

In order to produce H_2O_2 via Eq. (2) stability depends on factors such as cell configuration, cathode properties and operational conditions [18]. Wherein using undivided or divided electrochemical cells parasitic Reactions (5) and (6) can occur, diminishing the H_2O_2 accumulation in the system [19].

$$H_2O_2 + 2H^+ + 2e^- \rightarrow 2H_2O \quad (5)$$

$$2H_2O_2 \rightarrow O_{2(g)} + 2H_2O \quad (6)$$

The use of an undivided cell can propitiate H_2O_2 oxidation to oxygen at the anode according to Eqs. (7) and (8), producing the weak oxidant hydroperoxyl radical ($HO_2^\bullet$ $E^\circ(HO_2^\bullet/H_2O) = 1.65$ V/SHE) as intermediate [20].

$$H_2O_2 \rightarrow HO_2^\bullet + H^+ + e^- \quad (7)$$

$$HO_2^\bullet \rightarrow O_2 + H^+ + e^- \quad (8)$$

Carbon-based cathodes have been reported as being effective in H_2O_2 electrogeneration from Reaction (2) [21–24]. Supported metallic nanoparticles have been used to improve the catalytic activity of carbon for hydrogen peroxide electrogeneration [25–28]. Additionally, this materials can be used for gas diffusion electrodes (GDE) construction, which are very attractive for industrial and practical applications [29], and exhibit high efficiency in the *in-situ* generation of H_2O_2 via the oxygen reduction reaction maximizing the contact between cathode, oxygen and water [18].

The use of bimetallic nanostructures in the core-shell type has attracted considerable interest mainly on materials for alternative power devices due to their peculiar and versatile properties compared to the bulk metals and its corresponding monometallic particles [30]. In addition, coating a high cost metal (*e.g.*, Au, Pt or Pd) as a monolayer onto the surface of non-precious metal-based nanostructures (*e.g.*, Ni, Fe or Co) can reduce the cost and even increase the catalytic efficiency [31].

These nanostructures provide advantages including the possibility of core serves as a support for the shell, allowing the surface to present differential porosity and surface area, the synergism between the shell and the core contributes to a high efficiency/yield/selectivity in catalytic applications improving its performance [31].

Gold is known as a good catalyst for ORR mechanism via 2 electrons, with H_2O_2 as the major product, in acidic medium. Since its weak binding with O_2 and OOH the breaking of O-O bonds is not facilitated [32]. The use of supported Au nanoparticles employed as electrocatalysts for the ORR in aqueous solutions is attractive because it can contribute to an increase in H_2O_2 electrogeneration due to its interaction with oxygen in the energy conversion context [33,34].

Similarly, the tungsten catalytic activity in the oxygen reduction reaction is also already known. Assumpção et al. [25] investigated the behavior of tungsten trioxide (WO_3) as an electrocatalyst on the electrogeneration of H_2O_2 by ORR and verified that 1% of this oxide supported on carbon considerably increased the catalytic activity of the Vulcan carbon for this purpose. This material exhibits surface acidity due to the presence of Lewis-Brønsted acidic sites related to W^{6+} species presenting higher hydrophilicity and consequently has higher activity in the ORR for H_2O_2 production than the other materials used in that work.

For the reasons indicated above, the original approach of the application of core-shell type W@Au nanostructures may be promising for H_2O_2 electrogeneration. In this work, we report a facile strategy for the synthesis of W@Au structures, followed by a comparative study of two proportions of the core-shell nanoparticles supported on carbon (1% and 2%) as electrocatalysts for the ORR. The main goal of this paper was to understand how both the W@Au loading and structure affect the electrocatalytic activity of the Vulcan XC-72R carbon for peroxide electrogeneration.

2. Experimental

2.1. Materials and methods

Analytical grade chemicals WCl_4 (tungsten(IV) chloride, 95% Sigma–Aldrich), $Na_3C_6H_5O_7.2H_2O$ (sodium citrate dihydrate, 99%, Sigma–Aldrich), $NaBH_4$ (sodium borohydride, ReagentPlus®, 99.0%, Sigma–Aldrich), $HAuCl_4.3H_2O$ (gold(III) chloride trihydrate, 17% Au in HCl, Sigma–Aldrich), $C_6H_8O_6$ (ascorbic acid, 99.0%, BioXtra), NaOH (sodium hydroxide, Synth), H_2SO_4 (sulfuric acid, Synth), K_2SO_4 (potassium sulfate, Sigma-Aldrich) and Vulcan carbon XC-72R (Cabot Corporation) were used. All solutions were prepared using deionized water (18.2 MΩ).

Both samples were characterized by X-ray diffraction (XRD) using a D8 Focus, Bruker AXS diffractometer with Cu-Kα radiation (40 kV, 40 mA). All diffractograms were recorded from $2\theta = 20^\circ$ to 90° with a step size of 0.05° and a scan time of 2 s per step. Transmission Electron Microscopy (TEM) images were obtained with a JEOL microscope JEM-2100 operated at 200 kV equipped with energy-dispersive spectrometer (EDS) using a Cu grid as specimen support. Using a Varian Cary 50 Bio spectrophotometer, UV–Vis spectra were recorded from aqueous suspensions containing the nanostructures and the H_2O_2 produced by the GDE.

The XPS analysis was performed at a pressure of less than 10^{-7} Pa using a commercial spectrometer (UNI-SPECS UHV System). The Al-Kα line was used ($h\nu = 1486.6$ eV), and the analyzer pass energy was set to 10 eV. The inelastic background of the Au 4f and W 4f electron core-level spectra was subtracted using Shirley's method. The composition (at. %) of the near surface region was determined with an accuracy of ±10% from the ratio of the relative peak areas corrected by Scofield's sensitivity factors of the corresponding elements. The spectra were fitted without placing constraints using multiple Voigt profiles.

Contact angle measurements of W@Au/C materials were performed using a GBXTM digidrop autogoniometer to characterize their wettability. For this purpose, dispersions of each sample containing 6 mg of the W@Au/C material mixed in 6 mL of water were prepared and then sonicated for 60 min in an ultrasonic bath. An aliquot of 50 μL of the dispersion was placed onto a glassy carbon electrode and then dried with a nitrogen flow to form a thin layer used as a substrate. A drop of 5 μL of pure water was added to the carbon substrate formed to determine the contact angle and its standard deviation. Measurements were taken every minute over a period of 5 minutes for each material, and the measurements were performed in triplicate.

2.2. Synthesis of W@Au structures

The W@Au 1% (0.5 wt% W + 0.5 wt% Au) and 2% (1 wt% W + 1 wt% Au) nanoparticles were prepared as described by Silva et al. [35]. First, the WCl_4 salt was dissolved in 25 mL of H_2O and the solution was heated to 90 °C under stirring. Thereafter, 5 mL of sodium citrate solution was added at the same molar ratio of WCl_4 solution, and then a further 5 mL of a solution of $NaBH_4$ (4 times the molar ratio of WCl_4) was dissolved in cold water. At this point, the solution was removed and an instantaneous spectrum of the solution was obtained in the UV-Vis, with a subsequent decrease of the temperature to 40 °C. 1% and 2% of Au/Vulcan XC72R were also prepared in order to compare the activity for peroxide formation using the rotating ring-disk technique with the core-shell structures. These two proportions were prepared using the same procedure above (for core-shell nanostructures) but with only one reduction step.

A solution of $HAuCl_4$ was separately prepared with ascorbic acid in the molar ratio 1:1, and then the W solution was added to the Au solution before obtaining a new UV–vis absorption spectrum. The mixture was heated to 70 °C, maintaining this temperature while stirring for 1 hour. After this period of stirring, another UV–Vis spectrum was taken. Subsequently, the material was centrifuged for 15 minutes at 4500 rpm.

2.3. Preparation of the W@Au/C electrocatalyst

Preparation of the W@Au/C electrocatalyst consisted of forming the mixture of a predetermined volume of synthesized nanoparticles containing solution with 0.2 g of Vulcan carbon XC-72R (1 and 2% w/w). This mixture was placed in an ultrasonic bath for over 60 min under vigorous stirring and then dried at 350 °C for 1 h in an N_2 atmosphere.

2.4. Electrochemical measurements

Electrochemical measurements were conducted based on the polarization curves at steady state obtained using a potentiostat/galvanostat Autolab PGSTAT 302N and a rotating ring-disk commercial electrode from Pine Instruments, with a central glassy carbon disk (area = 0.2475 cm^2) and a gold ring (0.1866 cm^2), with a collection efficiency of N = 0.28 (experimental) and N = 0.22 (theoretical). The electrode rotation speed was varied between 100 and 3600 rpm. The employed electrolyte was NaOH 1 mol L^{-1}, and all measurements were performed in duplicate.

In addition, a conventional electrochemical cell was used to perform electrochemical measurements; the cell consists of 3 compartments, with a capacity of 20 mL of solution, wherein the reference electrode was Hg/HgO, the counter electrode was platinum wire, and the working electrode was prepared as described by Paulus *et al.* [36]. Dispersions with 5 mg of the electrocatalyst were prepared in 5 mL water and then homogenized in an ultrasonic bath for 60 minutes. After homogenization, an aliquot of 20 μL of the solution is inserted into the disk electrode and then dried by N_2 flow. Subsequently, 20 μL of diluted Nafion ® Sigma–Aldrich 15 to 20% water Perfluorinated resin solution – 5% lower aliphatic alcohols and water solution (1:100 v/v Nafion: water) was added over the electrocatalyst layer, and again dried by N_2 flow to form a thin layer.

2.5. Manufacture of the gas diffusion electrodes

Gas diffusion electrodes of the material that showed higher catalytic activity for the ORR were prepared. Initially, the synthesis of 6 grams of material was performed as described in Sections 2.2 and 2.3. The powder was transferred to a beaker and then approximately 100 mL of distilled water was added. Stirring was maintained at 400 rpm for 30 minutes and, if necessary, additional water was added to form a homogeneous solution. Polytetrafluoroethylene Teflon® PTFE TE 3859 (60% dispersion), which acts as binding agent, was weighed to 20% of the final mass of the material with respect to the weight of the electrocatalyst, i.e., (1% (w/w) W@Au/C) and 20% w/w of a 60% aqueous dispersion of DuPont. The PTFE was added to the solution and stirring was maintained for one hour. Finally, the mixture was filtered under vacuum and then dried in an oven at 110 °C for 30 minutes.

The GDE was synthesized in a circular shape mold with a 2.5 cm diameter. First, a metallic plate was placed in the mold, then 2.0 grams of the prepared electrocatalyst was added, and finally another stainless steel plate was placed on top. The material was then compressed with 2 tons for two hours, maintaining the mold temperature at 290 °C. The electrode was removed from the mold when it reached room temperature.

2.6. H_2O_2 quantification using gas diffusion electrodes

To quantify the H_2O_2 electrogeneration using the GDE, exhaustive electrolysis tests were performed by applying different potentials, as proposed by Forti *et al.* [37]. The experiments were performed in an electrochemical cell with a capacity of 350 mL using the GDE as the working electrode. The reference and counter electrode were commercial Ag/AgCl and platinum (pure platinum screen), respectively. The employed electrolyte was 0.1 M H_2SO_4 + 0.1 M K_2SO_4, and the electrolyte was previously saturated with oxygen for 40 minutes. The O_2 flow (0.2 bar) was maintained throughout the experiment. Furthermore, during electrolysis, aliquots of 500 μL were withdrawn and added to 4 mL of ammonium molybdate solution 2.4×10^{-3} mol L^{-1} in sulfuric acid (0.5 mol L^{-1}) to form peroxy molybdate, a complex that is yellow in color. These solutions were then analyzed in a Varian spectrophotometer Cary 50 at the wavelength of 350 nm to determine the concentration of H_2O_2 produced. For this analysis, an analytical curve was previously made.

3. Results and discussion

3.1. Physical-chemical characterization

UV–Vis spectroscopy was used to investigate the existence of the layer of Au over W particles. In Fig. 1, the UV–Vis absorption spectra of WCl_4 (black line) and $HAuCl_4$ (red line) are presented. The spectrum of Au solution showed the presence of a peak located at approximately 320 nm. Studies indicate that, when the metal responsible for forming the shell is added during the synthesis of the core-shell type structures, a change in the spectrum obtained occurs, i.e., a reduction of the peaks of the material that comprising the core and the appearance of peaks characteristic of the material consisting of the outer portion [38].

Note that after the mixing of the solutions, the final nanoparticle solution presented a large decrease of the peak at 320 nm and showed a plasmon band resonance shifted to higher wavelengths (580 nm, Fig. 1 blue line), in agreement with the formation of a gold shell and an increase of the Au structure size [39–41].

Fig. 2a shows a TEM image of the 1% W@Au/C electrocatalyst, indicating that the particles had spherical shape with a diameter of approximately 100 nm. The two colors clearly observed suggest the formation of core-shell type structure. Fig. 2b shows the EDS spectrum of 1% W@Au/C electrocatalyst prepared via the chemical reduction method. The result of EDS shows that the composites prepared consist of Cu, Au and W at the noise level (as expected for

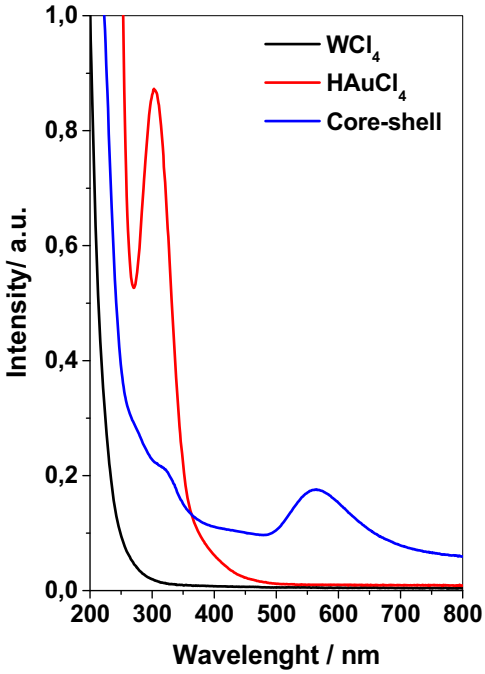

Fig. 1. UV-Vis spectra obtained during the synthesis steps (see Section 2.2). (For interpretation of the references to colour in the text, the reader is referred to the web version of this article.)

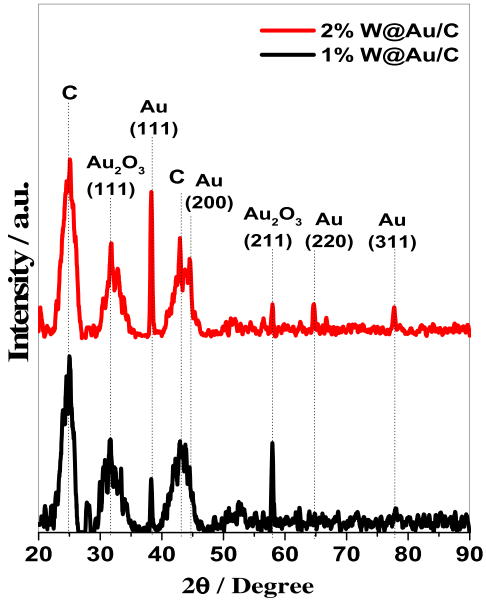

Fig. 3. XRD patterns of electrocatalysts based on W@Au/C 1% and 2% supported on Vulcan Carbon XC-72R.

a core-shell type structure), according to the TEM image. The Cu peak is related to TEM grid used as specimen support.

The crystal planes of the nanostructured materials were obtained by XRD analysis and are presented in Fig. 3. Four diffraction peaks positioned at 38.1, 44.5, 64.6, and 77.7° are indexed to the (111), (200), (220) and (311) diffraction peaks of metallic Au (JCPDS no. 04-0784), respectively. This result confirmed that the Au nano-structures formed are of highly crystalline nature. The diffraction peaks located at 31.5 and 58.2° are the characteristic peaks of Au_2O_3 (JCPDS no. 43-1039), and the peaks obtained at 24.6° and 43.2° are assigned to the diffraction peaks of carbon.

The detection of Au phases and the lack of detection of tungsten phases is further evidence of the core-shell type structure formation, indicating that tungsten has been covered by gold.

There are reports in the literature stating that the Au_2O_3 phase has oxygen vacancies in its structure [42] and interstitial oxygen atoms, which are easier to remove. At the same time, it has been reported that because of oxygen vacancies, the diffusion in non-stoichiometric metal oxides is faster compared to diffusion in stoichiometric oxides [43,44]. Furthermore, the Au_2O_3 phase is very relevant in relation to the active sites of the catalyst because, as observed in some metal oxides, the presence of oxygen vacancies is due to defects in the crystal structure [42]. Assumpção *et al.* [16] observed, in their studies of materials based on CeO_2/C, that they had oxygen vacancies (not stoichiometric ceria) acting as an oxygen buffer in the reaction medium. This particularity provided an increase in oxygen diffusion and consequently resulted in high H_2O_2 electrogeneration from ORR.

The quantitative XPS analysis confirmed a electrocatalyst loading of 1 and 2 wt% in the carbon matrix, indicating a similar atomic concentration of Au and W in both samples of approximately 0.1 and 0.2 at.%, respectively, being close to the detection

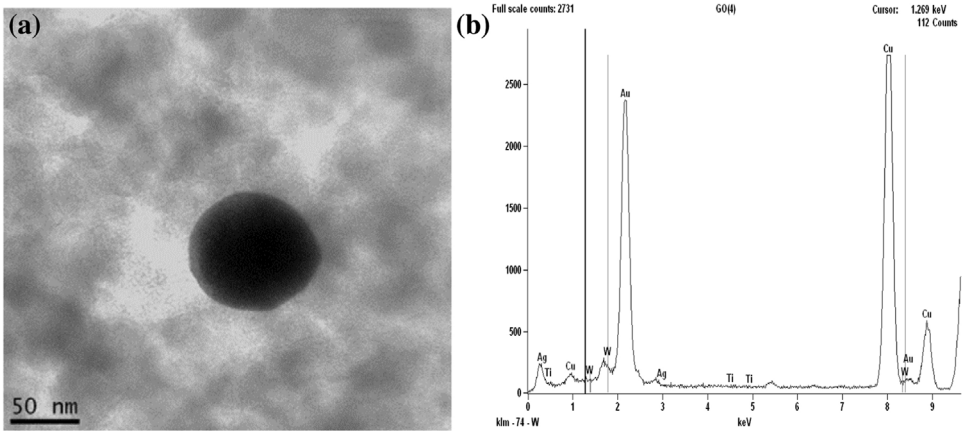

Fig. 2. a) TEM images of 1% W@Au/C electrocatalyst and b) EDS spectrum of 1% W@Au/C prepared.

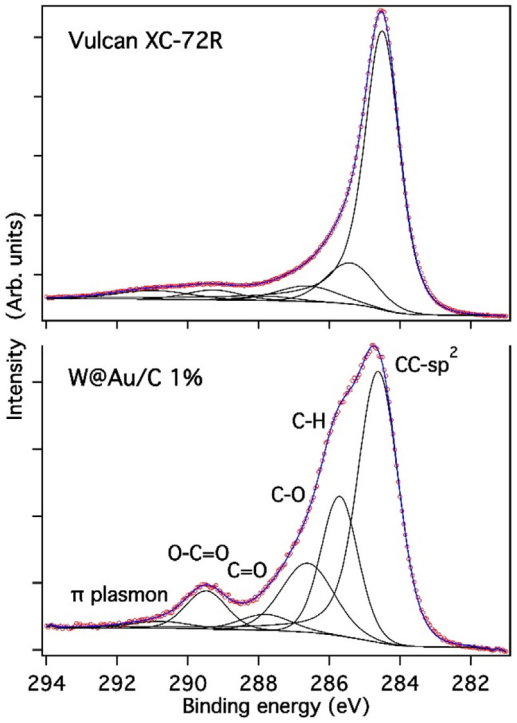

Fig. 4. Deconvoluted XPS C 1s spectra of the W@Au/C 1% electrocatalysts and the Vulcan XC-72R support.

limit of the technique. For Vulcan XC-72R, an oxygen content of 3.0 at.% was determined, while for the W@Au/C samples, the oxygen content increased to 13.5 at.%. The deconvoluted C 1s spectra shown in Fig. 4 indicate that the oxygenated carbon of W@Au/C catalysts consists mainly of ether/alcohol groups (61%) and contains, to a lesser extent, carboxyl (29%) and carbonyl groups (10%).

Table 1
Average values of contact angles of the carbon support and electrocatalysts.

Substrate	Contact angle (°)
Vulcan XC-72R	57 ± 1
W@Au/C 1%	45 ± 3
W@Au/C 2%	27 ± 2

Despite the low signal-to-noise ratio, the deconvolution of the Au 4f and W 4f high-resolution spectra allowed for identification of the phases present in the electrocatalyst. As can be inferred from the fitted spectra in Fig. 5, the Au 4f spin-orbit pair was deconvoluted into two components, indicating the presence of metallic Au and Au_2O_3 phases. Note that the fraction of the oxide phase increased from approximately 12% to 28% as the catalyst loading was decreased from 2 to 1 wt%. The W 4f spectra were fitted with good precision using one spin-orbit pair, attributed to the WO_3 phase [45].

Both the 1% and 2% W@Au supported on Vulcan carbon showed smaller contact angles than Vulcan XC-72R (45° and 27°, respectively), as can be observed in the average contact angles given in Table 1, indicating that these substrates have a higher hydrophilicity. The presence of oxygenated acids species in higher quantities in nanostructured material as it can be seen in XPS analysis may provide greater hydrophilicity to the material which may contribute to an increase in H_2O_2 electrogeneration. The occurrence of oxygenated acid species in the electrocatalyst surface may have contributed to the increased carbon hydrophilic character [46], which, despite a very high concentration of these species, can decrease the carbon conductivity; therefore, the material has a lower catalytic activity as 2% W@Au/C [29]. These properties were investigated by XPS analyses.

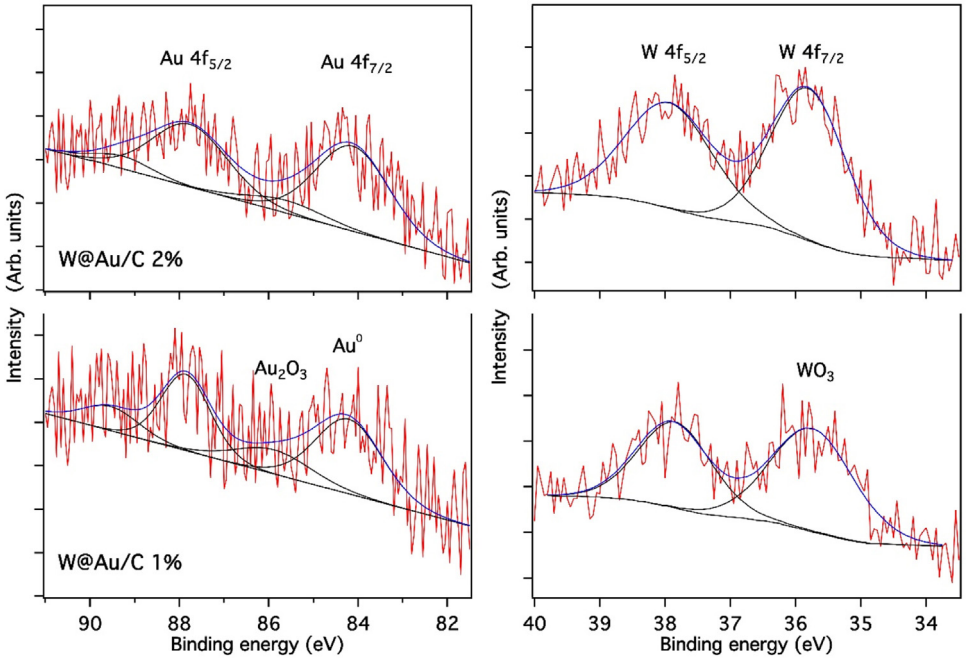

Fig. 5. Deconvoluted XPS Au 4f and W 4f spectra of the electrocatalysts supported on Vulcan XC-72R.

The addiction of nanostructures increases the surface area of the catalyst favoring an increasing in the number of species adsorbed. There is a change in the mean electronic properties of core-shell in very small particles suggesting that the binding energy is changed due or not due to interactions with the carbon support, which can justify a change of the adsorption and catalysis properties [47].

It is important to point out that the form of the adsorption of the oxygen molecules at the core-shell carbon modified surface with the increasing in the hydrophilicity was modified. It is suggested that the Pauling Model of adsorption of oxygen molecules is favored; in this case there is no breaking of the oxygen-oxygen bond favoring the formation of hydrogen peroxide.

3.2. Electrochemical measurements

The activity of the W@Au electrocatalysts was evaluated by the technique of rotating ring-disk via the polarization curves at steady state; the results are shown in Fig. 6. The polarization curve results of Vulcan XC-72R and Pt/C E-TEK, reference materials for ORR via 2-electron and 4-electron reduction, respectively, are also shown for comparison.

The electrochemical measurements were performed in oxygen-saturated 1 mol L^{-1} NaOH at a scan rate of 5 mV s^{-1} and 1600 rpm electrode rotation. The polarization curves for pure Vulcan XC-72R and Pt/C E-TEK are also shown for comparison.

The disk polarization curves for the ORR using materials based on W@Au/C presented current values close to those for carbon Vulcan XC-72R and smaller values compared to those for the platinum disk. This result indicates the transfer of 2 electrons in ORR. Considering both of the electrocatalysts containing W@Au/C materials, the material with 1% loading showed the highest ring current for ORR (ring held at 0.2 V), which corresponds to the highest rate of production of H_2O_2. The decreasing order of catalytic activity for peroxide formation taking into account ring currents values was 1% W@Au/C > 1% Au/C > 2% Au/C > 2% W@Au/C > Vulcan XC72R. For this reason, 1% W@Au/C was used for the production of hydrogen peroxide using Gas Diffusion Electrodes (GDE) comparing with Vulcan XC72R, Fig. 7.

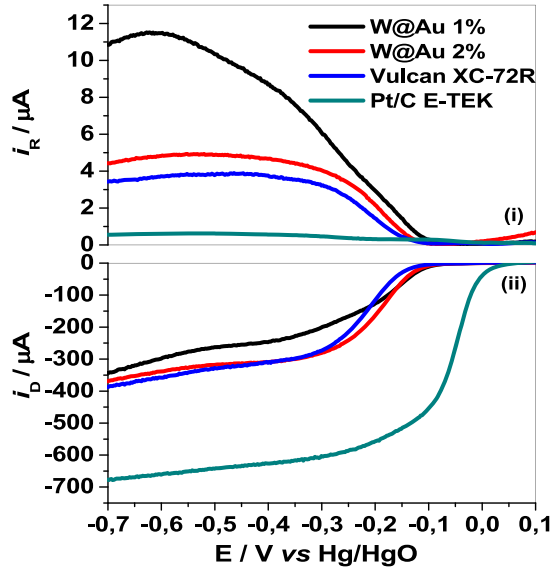

Fig. 6. Steady-state polarization curves for the ORR of different proportions of W@Au supported on Vulcan XC-72R carbon. Current were measured at the glassy carbon disk electrode. Black – 1% W@Au/C, Red – 2% W@Au/C, Blue – Vulcan XC72R and Cyan – Pt/C Etek. (For interpretation of the references to colour in this figure legend, the reader is referred to the web version of this article.)

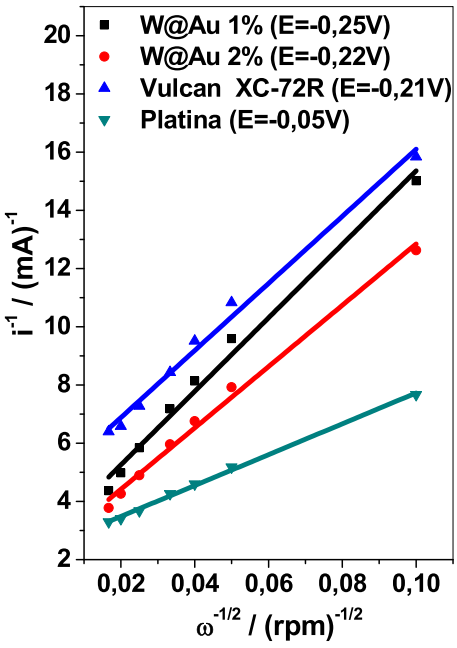

Fig. 7. Koutecky–Levich plots for ORR on W@Au based materials in 1 mol L^{-1} NaOH. The plots for Vulcan XC-72R and Pt/C E-TEK are also shown for comparison.

In a rotating ring-disk experiment, the measured current (i) may be limited primarily by two phenomena: the mass transport of the electroactive species to the electrode surface, which defines the diffusion current (i_d); and the electron transfer between the surface and the electroactive species, which defines the kinetic current (i_k). In mathematical terms, this observation may be represented by the Koutecky-Levich equation (Eq. (9)).

$$\frac{1}{i} = \frac{1}{i_d} + \frac{1}{i_k} \tag{9}$$

The kinetic and diffusion currents can be expressed by Eqs. (10) and (11), respectively:

$$i_d = 0.20\, n\, F\, A\, D_{O_2}^{2/3} \nu^{-1/6} C^0 \omega^{1/2} \tag{10}$$

$$i_k = n\, F\, A\, k\, C^0 \tag{11}$$

where n is the number of transferred electrons, F is Faraday's constant (96487C mol^{-1}), A is the area effectively covered with the catalyst, D_{O2} is the oxygen diffusion coefficient, ν is the kinematic viscosity electrolyte ($cm^2\, s^{-1}$), C^0 is the saturated oxygen concentration in the solution, ω is the angular rotational speed of the electrode (rpm) and k is a constant of electron transfer rate ($cm^3\, mol^{-1}\, s^{-1}$).

Insertion of the expression (10) into Eq. (9) leads to Eq. (12), where $B = 0.20\, n\, F\, A\, D_{O_2}^{2/3} \nu^{-1/6} C^0$.

$$\frac{1}{i} = (1/B)\frac{1}{\omega^{1/2}} + \frac{1}{i_k} \tag{12}$$

Thus, the Koutecky-Levich graph (i^{-1} versus $\omega^{-1/2}$) results in a straight line, whose value of the slope (1/B) provides an estimate of the number of electrons involved in the electrochemical process at a given potential. Therefore, the plots of Eq. (12) for all electrocatalysts are shown in Fig. 7.

Parallel straight lines were obtained using the Koutecky-Levich equation for materials based on W@Au. The slope of these lines is directly proportional to the number of electrons exchanged for these catalysts in the ORR. The slope of the line using the electrocatalyst W@Au/C 1% (126 $(rpm)^{-1/2}$ $(mA/cm^2)^{-1}$) is near to the value obtained for Vulcan carbon XC-72R (115 $(rpm)^{-1/2}$ $(mA/cm^2)^{-1}$), suggesting the transfer of 2 electrons for ORR by the W@Au based material. The straight slope obtained for the platinum-based material in the same process was 53 $(rpm)^{-1/2}$ $(mA/cm^2)^{-1}$.

Assuming that the ORR on carbon catalysts produces H_2O_2 mainly through the transfer of two electrons per molecule of oxygen for the ring-disk experiments used in this study, the number of moles of electrons involved in the reduction of 1 mol of oxygen by W@Au/C 1% catalyst is also expected to be close to 2.

The amount of H_2O_2 electrogenerated by the Vulcan XC-72R carbon GDE and by the 1% W@Au/C GDE (best material according to ring-disk experiments) was analyzed and the results are shown in Fig. 8a and b, respectively, as a function of the electrolysis time at different applied potentials. The production of H_2O_2 was quantified using a calibration curve, which was performed over a concentration range of 50–700 mg L^{-1} of H_2O_2 ($[H_2O_2] = (0.01067 + Abs)/0.0014$, $R = 0.999$).

It was found that the best potential for H_2O_2 electrogeneration on 1% W@Au/C material was −1.1 V, at which 120 ppm of H_2O_2 was produced, while Vulcan XC-72R GDE produced 83 ppm at the same potential. Thus, the use of 1% of core-shell W@Au type nanostructures supported on carbon was able to increase the electrogeneration of hydrogen peroxide by nearly 50%. Above or below this potential value, a decrease in the H_2O_2 production was observed. An increase of the applied potential may favor the ORR via the 4-electron mechanism, where the main product is H_2O, which could explain the reduction of generated H_2O_2.

The results of H_2O_2 electrogeneration are in agreement with the results obtained using the rotating ring-disk electrode technique, which showed that the electrocatalyst based on 1% W@Au/C presented the highest ring current, indicating higher H_2O_2 generation. The experiments involving exhaustive electrolysis using GDE in the electrochemical cell confirmed the highest generation of H_2O_2 using this material.

All electrochemical measurements indicated that the electrocatalyst based on 1% W@Au/C is a promising material for H_2O_2 electrogeneration and consequently can be applied on AOPs on the degradation of organic pollutants in water. It is important to stress that the electrocatalysts here prepared have equal or better production of hydrogen peroxide than those ones previously reported by our group [16,25].

A possible explanation for the behavior observed can be discussed using five important points: (1) the gold surface presents differential porosity, surface area and increased presence of the Au_2O_3 phase, thus, resulting in a high catalytic activity; (2) the synergism between the shell and the core contributes to a great efficiency/yield/selectivity in H_2O_2 electrogeneration; (3) the combination of the core and shell properties contribute to the performance improvement; (4) the two elements are consistent for H_2O_2 formation; and (5) the presence of oxygenated acid carbon species, as detected by XPS, results in an increase of the hydrophilicity of the surface (as measured by contact angles measurements), thereby increasing the conductivity. In other words, the presence, even at an ultra-low amount (1%), of core-shell type structures modifies the carbon surface.

4. Conclusions

Regarding the results of the rotating ring-disk electrode, the W@Au/C based materials showed an improvement in the electrocatalytic activity compared to pure carbon and to commercial platinum in the electrogeneration of H_2O_2. The two proportions tested (1 and 2%) have higher ratios of ring current values, in which the maximum activity was detected for 1% loading.

H_2O_2 electrogeneration analysis using GDE based on the material 1% W@Au/C showed that this electrocatalyst can generate nearly 50% more hydrogen peroxide than the Vulcan XC-72R carbon GDE. These results could be explained based on the favorable synergistic interactions between the W (core) and Au (shell) that result in increased catalytic activity. Furthermore, XPS results showed that, besides the observed increase of the oxygenated groups of the carbon support containing the catalyst nanoparticles, the 1% W@Au/C sample contains a higher fraction the Au_2O_3 phase, leading to an overall higher activity of this

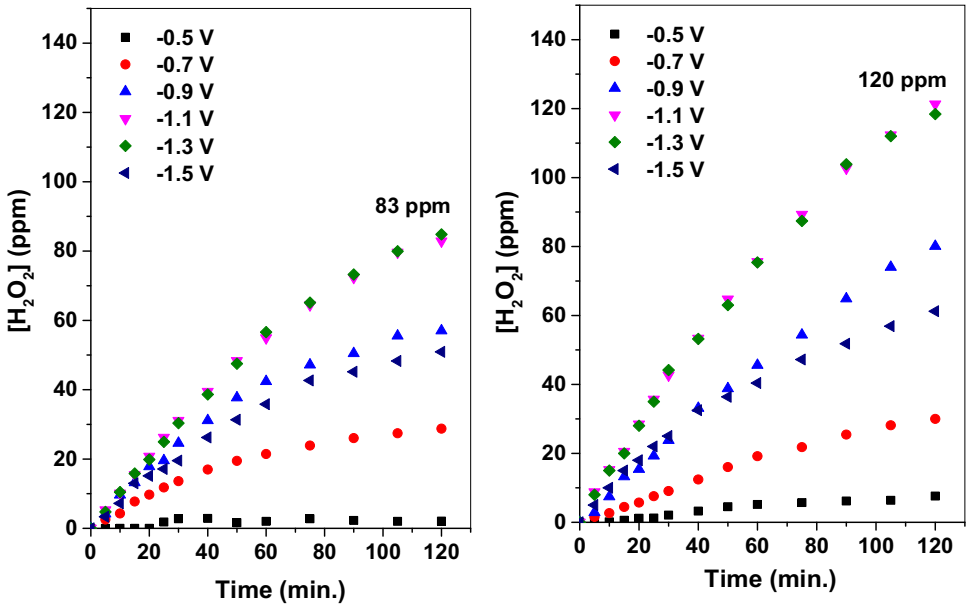

Fig. 8. H_2O_2 concentration as a function of electrolysis time using a) Vulcan XC-72R GDE and b) W@Au/C 1% GDE. Supporting electrolyte: 0.1 M H_2SO_4 + 0.1 M H_2SO_4. O_2 flow = 0.2 bar.gr8

electrocatalyst. The reduction of the cost of the electrocatalyst is an important issue; because of the very small amount of gold used in the synthesis for the formation of the thin gold layer on the tungsten core, the catalyst features an excellent price-performance ratio.

Acknowledgements

The authors thank Almir Oliveira Neto from IPEN for performing the TEM and EDS analyses. M.C. Santos is grateful to CNPq (grant numbers: 474913/2012-0, 406612/2013-7), CAPES, Instituto Nacional de Ciência e Tecnologia (INCT) Energia e Meio Ambiente (Process Number: 573.783/2008-0) and FAPESP (Process Number: 2015/10314-8) for their financial support. V.S. Antonin thanks her Doctoral fellowship from FAPESP (grant number: 2011/21656-6). L. S. Parreira also acknowledges her Doctoral fellowship from FAPESP (grant number: 2011/00008-2).

References

[1] B.A. Wols, D.J.H. Harmsen, J. Wanders-Dijk, E.F. Beerendonk, C.H.M. Hofman-Caris, Water Res. 75 (2015) 11.
[2] J. Lian, Z. Qiang, M. Li, J.R. Bolton, J. Qu, Water Res. 75 (2015) 43.
[3] M.G. Alalm, A. Tawfik, S. Ookawara, J. Environ. Chem. Eng. 3 (2015) 46.
[4] R. Salazar, S. Garcia-Segura, M.S. Ureta-Zañartu, E. Brillas, Electrochim. Acta 56 (2011) 6371–6379.
[5] E. Brillas, C.A. Martinez-Huitle, Appl. Catal B-Environ. 166–167 (2015) 603.
[6] M. Jović, D. Manojlović, D. Stanković, B. Dojčinović, B. Obradović, U. Gašić, G. Roglić, J. Hazard. Mater. 260 (2013) 1092.
[7] O. García, E. Isarain-Chávez, A. El-Ghenymy, E. Brillas, J.M. Peralta-Hernández, J. Electroanal. Chem. 728 (2014) 1.
[8] V.S. Antonin, M.C. Santos, S. Garcia-Segura, E. Brillas, Water Res. 83 (2015) 31.
[9] V.S. Antonin, S. Garcia-Segura, M.C. Santos, E. Brillas, J. Electroanal. Chem. 747 (2015) 1.
[10] I. Sirés, N. Oturan, M.A. Oturan, Water Res. 44 (2010) 3109.
[11] A. Thiam, I. Sirés, E. Brillas, Water Res. 81 (2015) 178.
[12] I. Yamanaka, T. Hashimoto, R. Ichihashi, K. Otsuka, Electrochim. Acta 53 (2008) 4824.
[13] J.M. Campos-Martin, G. Blanco-Brieva, J.L.G. Fierro, Angew. Chem. Int. Ed. 45 (2006) 6962.
[14] G. Xia, Y. Lu, H. Xu, Electrochim. Acta 158 (2015) 390.
[15] Y. Sheng, S. Song, X. Wang, L. Song, C. Wang, H. Sun, X. Niu, Electrochim. Acta 56 (2011) 8651.
[16] M.H.M.T. Assumpção, A. Moraes, R.F.B. De Souza, I. Gaubeur, R.T.S. Oliveira, V.S. Antonin, G.R.P. Malpass, R.S. Rocha, M.L. Calegaro, M.R.V. Lanza, M.C. Santos, Appl. Catal. A-Gen. 411–412 (2012) 1.
[17] F.L. Silva, R.M. Reis, W.R.P. Barros, R.S. Rocha, M.R.V. Lanza, J. Electroanal. Chem. 722–723 (2014) 32.
[18] F.C. Moreira, R.A.R. Boaventura, E. Brillas, V.J.P. Vilar, Appl. Catal. B- Environ. 202 (2017) 217.
[19] A.A. Gallegos, Y.V. García, A. Zamudio, Sol. Energy Mater. Sol. Cells 88 (2005) 157.
[20] E. Brillas, R.M. Bastida, E. Llosa, J. Casado, J. Electrochem. Soc. 142 (1995) 1733.
[21] B. Balci, N. Oturan, R. Cherrier, M.A. Oturan, Water Res. 2009 (1924) 43.
[22] A. Dhaouadi, N. Adhoum, J. Electroanal. Chem. 637 (2009) 33.
[23] I. Sirés, C. Arias, P.L. Cabot, F. Centellas, J.A. Garrido, R.M. Rodríguez, E. Brillas, Chemosphere 66 (2007) 1660.
[24] A.R. Khataee, M. Zarei, S.K. Asl, J. Electroanal. Chem. 648 (2010) 143.
[25] M.H.M.T. Assumpção, R.F.B. De Souza, R.M. Reis, R.S. Rocha, J.R. Steter, P. Hammer, I. Gaubeur, M.L. Calegaro, M.R.V. Lanza, M.C. Santos, Appl. Catal. B Environ. 142–143 (2013) 479.
[26] M.H.M.T. Assumpção, A. Moraes, R.F.B. De Souza, M.L. Calegaro, M.R.V. Lanza, E. R. Leite, M.A.L. Cordeiro, P. Hammer, M.C. Santos, Electrochim. Acta 111 (2013) 339.
[27] V.S. Antonin, M.H.M.T. Assumpção, J.C.M. Silva, L.S. Parreira, M.R.V. Lanza, M.C. Santos, Electrochim. Acta 109 (2013) 245.
[28] F.V.E. dos Reis, V.S. Antonin, P. Hammer, M.C. Santos, P.H.C. Camargo, J. Catal. 326 (2015) 100.
[29] E. Brillas, I. Sirés, M.A. Oturan, Chem. Rev. 109 (2009) 6570.
[30] M. Mazloum-Ardakani, L. Hosseinzadeh, Z. Taleat, Biosens. Bioelectron. 74 (2015) 30.
[31] M.B. Gawande, A. Goswami, T. Asefa, H. Guo, A.V. Biradar, Dong-Liang Peng, R. Zboril, R.S. Varma, Chem. Soc. Rev. 44 (2015) 7540.
[32] Y.L. Zheng, D. Mei, Y. Chen, S. Ye, Electrochem. Commun. 39 (2014) 19.
[33] H. Yin, H. Tang, D. Wang, Y. Gao, Z. Tang, ACS Nano 6 (2012) 8288.
[34] P. Quaino, N.B. Luque, R. Nazmutdinov, E. Santos, W. Schmickler, Angew. Chem. Int. Ed. 51 (2012) 12997.
[35] J.C.M. Silva, R.F.B. De Souza, L.S. Parreira, E. Teixeira Neto, M.L. Calegaro, M.C. Santos, Appl. Catal. B-Environ. 99 (2010) 265.
[36] U.A. Paulus, T.J. Schmidt, H.A. Gasteiger, R.J. Behm, J. Electroanal. Chem. 495 (2001) 134.
[37] J.C. Forti, R.S. Rocha, M.R.V. Lanza, R. Bertazzoli, J. Electroanal. Chem. 602 (2007) 63.
[38] X. Li, J. Liu, W. He, Q. Huang, H. Yang, J. Colloid Interf. Sci. 344 (2010) 132.
[39] L. Minati, C.L. Cheng, Y.C. Lin, J. Hees, G. Lewes-Malandrakis, C.E. Nebel, F. Benetti, C. Migliaresi, G. Speranza, Diam. Relat. Mater. 53 (2015) 23.
[40] R. Feng, M. Li, J. Liu, Colloid. Surface. A 406 (2012) 6.
[41] R. Liu, H. Chen, S. Hu, China Particuology 2 (2004) 160.
[42] X. He, H. Yang, J. Mol. Catal. A-Chem. 379 (2013) 219.
[43] G. Zhou, P.R. Shah, T. Montini, P. Fornasiero, R.J. Gorte, Surf. Sci. 601 (2007) 2512.
[44] B. Rotavera, A. Kumar, S. Seal, E.L. Petersen, Proc. Combust. Inst. 32 (2009) 811.
[45] AV. Naumkin, A. Kraut-Vass, S.W. Gaarenstroom, C.J. Powell, NIST X-ray Photoelctron Spectroscopy Database, NIST Standard Reference Database 20, v. 4.1: http://srdata.nist.gov/XPS/ and the references within.
[46] M.H.M.T. Assumpção, R.F.B. De Souza, D.C. Rascio, J.C.M. Silva, M.L. Calegaro, I. Gaubeur, T.R.L.C. Paixão, P. Hammer, M.R.V. Lanza, M.C. Santos, Carbon 49 (2011) 2842.
[47] L. Geniès, R. Faure, R. Durand, Electrochimica Acta 44 (1998) 1317.